Tropospheric nitric acid columns from the IASI satellite instrument interpreted with a chemical transport model: Implications for parameterizations of nitric oxide production by lightning

Matthew Cooper, Randall V. Martin, Catherine Wespes, Pierre-François Coheur, Cathy Clerbaux, Lee T. Murray

AGU PUBLICATIONS

JGR

Journal of Geophysical Research: Atmospheres

RESEARCH ARTICLE
10.1002/2014JD021907

Key Points:
- Tropospheric HNO_3 columns inferred from IASI using information from GEOS-Chem model
- GEOS-Chem underestimates tropospheric HNO_3 in Southeast Asia
- Treatment of lightning NO_x is the most significant contributor to model bias

Correspondence to:
M. Cooper,
cooperm2@dal.ca

Citation:
Cooper, M., R. V. Martin, C. Wespes, P.-F. Coheur, C. Clerbaux, and L. T. Murray (2014), Tropospheric nitric acid columns from the IASI satellite instrument interpreted with a chemical transport model: Implications for parameterizations of nitric oxide production by lightning, *J. Geophys. Res. Atmos.*, *119*, 10,068–10,079, doi:10.1002/2014JD021907.

Received 14 APR 2014
Accepted 12 AUG 2014
Accepted article online 15 AUG 2014
Published online 27 AUG 2014

Tropospheric nitric acid columns from the IASI satellite instrument interpreted with a chemical transport model: Implications for parameterizations of nitric oxide production by lightning

Matthew Cooper[1], Randall V. Martin[1,2], Catherine Wespes[3], Pierre-Francois Coheur[3], Cathy Clerbaux[3,4], and Lee T. Murray[5]

[1]Department of Physics and Atmospheric Science, Dalhousie University, Halifax, Nova Scotia, Canada, [2]Harvard–Smithsonian Center for Astrophysics, Cambridge, Massachusetts, USA, [3]Spectroscopie de l'Atmosphère, Chimie Quantique et Photophysique, Université Libre de Bruxelles, Brussels, Belgium, [4]Sorbonne Universités, UPMC Univ. Paris 06; Université Versailles St-Quentin; CNRS/INSU, LATMOS-IPSL, Paris, France, [5]NASA Goddard Institute for Space Studies and Lamont-Doherty Earth Observatory, Columbia University, New York, New York, USA

Abstract This paper interprets tropical tropospheric nitric acid columns from the Infrared Atmospheric Sounding Interferometer (IASI) satellite instrument with a global chemical transport model (GEOS-Chem). GEOS-Chem and IASI columns generally agree over the tropical ocean to within 10%. However, the GEOS-Chem simulation underestimates IASI nitric acid over Southeast Asia by a factor of 2. The regional nitric acid bias is confirmed by comparing the GEOS-Chem simulation with additional satellite (High Resolution Dynamics Limb Sounder, Atmospheric Chemistry Experiment Fourier Transform Spectrometer) and aircraft (Pacific Exploratory Mission (PEM)-Tropics A and PEM-West B) observations of the middle and upper troposphere. This bias appears to be driven by the lightning NO_x parameterization, both in terms of the magnitude of the NO_x source and the ozone production efficiency of concentrated lightning NO_x plumes. We tested a subgrid lightning plume parameterization and found that an ozone production efficiency of 15 mol/mol in lightning plumes over Southeast Asia in conjunction with an additional 0.5 Tg N would reduce the regional nitric acid bias from 92% to 6% without perturbing the rest of the tropics. Other sensitivity studies such as modified NO_x yield per flash, increased altitude of lightning NO_x emissions, decreased convective mass flux, or increased scavenging of nitric acid required unrealistic changes to reduce the bias.

1. Introduction

Nitrogen oxides ($NO_x \equiv NO + NO_2$) in the free troposphere largely control the production of ozone (O_3), an important greenhouse gas and atmospheric oxidant. The dominant sink for NO_x is oxidation to nitric acid (HNO_3). HNO_3 is one of the main forms of reactive nitrogen (NO_y) in the free troposphere, representing up to 50% of NO_y in the tropical upper troposphere [*Kasibhatla et al.*, 1993; *Folkins et al.*, 2006]. However, models generally have difficulty reproducing observed NO_x/HNO_3 ratios [*Brunner et al.*, 2005; *Singh et al.*, 2007]. Improved understanding of HNO_3 production and loss mechanisms can help to better constrain NO_x emissions and in turn improve understanding of ozone production and its effect on climate.

Direct measurements of free tropospheric HNO_3 are rare, particularly in the tropics. HNO_3 measurements taken during aircraft campaigns offer high precision but have limited spatial and temporal coverage. Satellite instruments are capable of providing superior temporal and spatial sampling in the tropics. HNO_3 concentrations have been retrieved from observations from several satellite instruments, including Limb Infrared Monitor of the Stratosphere [*Gille et al.*, 1984], Michelson Interferometer for Passive Atmospheric Sounding [*Tsidu et al.*, 2005], Microwave Limb Sounder (MLS) [*Santee et al.*, 2004], Atmospheric Chemistry Experiment Fourier Transform Spectrometer (ACE-FTS) [*Wolff et al.*, 2008], and High Resolution Dynamics Limb Sounder (HIRDLS) [*Kinnison et al.*, 2008]. However, these instruments are primarily focused on high latitudes or stratospheric altitudes. In this study we use the Infrared Atmospheric Sounding Interferometer (IASI) instrument on the MetOp satellite platform. IASI is a high-resolution spectrometer that provides global observations of HNO_3 column abundances with an unprecedented spatial and temporal resolution [*Wespes et al.*, 2009].

Lightning NO_x has a large influence on tropospheric ozone and nitric acid, as lightning NO_x is emitted directly into the free troposphere where NO_x lifetimes are longer [*Liu et al.*, 1987; *Pickering et al.*, 1990; *Sauvage et al.*, 2007]. Best estimates of the global lightning NO_x source range from 2 to 8 Tg N a^{-1}, but significant uncertainty remains in both the magnitude and vertical and horizontal distribution of the source [*Martin et al.*, 2007; *Schumann and Huntrieser*, 2007]. A difficulty in modeling the effects of lightning NO_x is that lightning is a subgrid-scale process which must be parameterized in chemical transport models. Lightning parameterizations are most often based on meteorological properties and are sensitive to the convection scheme used in the model [*Tost et al.*, 2007; *Koshak et al.*, 2013]. Lightning NO_x production is often determined using a prescribed number of NO_x molecules produced per flash, but this value varies significantly between models [*Schumann and Huntrieser*, 2007]. O_3 and HNO_3 concentrations are sensitive to the vertical placement of lightning NO_x emissions [*Labrador et al.*, 2005]. Uncertainty also arises when considering the dispersion rate of lightning NO_x plumes as rates of chemical reactions vary nonlinearly with respect to NO concentrations [*Lin et al.*, 1988]. Since HNO_3 is highly soluble and is quickly scavenged in convective updrafts, HNO_3 concentrations are sensitive to convective mixing and wet deposition in models [*Giorgi and Chameides*, 1986; *Mari et al.*, 2000; *Staudt et al.*, 2003].

The following paper examines tropical tropospheric HNO_3 columns retrieved from IASI satellite measurements. Section 2 describes data sources and other tools used in this work. Section 3 describes GEOS-Chem, a state-of-the-science global chemical transport model that is used here to interpret the IASI observations. Section 4 describes how GEOS-Chem is used to investigate the ability of IASI to provide information about HNO_3 in the tropical troposphere. In the process of this evaluation, a bias in the GEOS-Chem HNO_3 simulation over the tropical West Pacific and Indian Oceans is discovered. Section 5 discusses several possible methods for resolving the bias, including changes to wet deposition and lightning processes.

2. Observational Data

IASI was launched on the MetOp satellite in October 2006, into a polar Sun-synchronous orbit with an equator crossing time of 9:30 A.M. and P.M. [*Clerbaux et al.*, 2009]. IASI is a nadir-viewing Fourier Transform Spectrometer measuring thermal infrared radiation between 645 and 2760 cm^{-1}. HNO_3 and CO profiles are retrieved with the Fast Operational/Optimal Retrievals on Layers for IASI processing chains set up by the Université libre de Bruxelles/Laboratoire Atmosphères, Milieux, Observations Spatiales (ULB/LATMOS) groups [*Hurtmans et al.*, 2012]. The IASI HNO_3 retrievals have ~1 degree of freedom of signal (DOFS) providing a total column for HNO_3 offering no vertical information, except in the tropics where the DOFS reaches 1.5 [*Wespes et al.*, 2009; *Hurtmans et al.*, 2012]. IASI provides global coverage twice daily. Both day and night observations are used here. IASI scans across track either side of the nadir, with a total swath of around 2000 km. Each field of view is composed of four circular pixels of 12 km diameter at nadir. IASI's vertical sensitivity to HNO_3 is largest in the upper troposphere and lower stratosphere (approximately between 15 and 30 km) with weak sensitivity near the surface. The lower tropospheric sensitivity is stronger in the tropics than in middle and polar latitudes because of higher surface temperatures [*Clerbaux et al.*, 2009]. Evaluation of previous IASI HNO_3 columns indicates average errors ranging from 12% at middle to high latitudes up to 32% near the equator [*Wespes et al.*, 2009; *Hurtmans et al.*, 2012]. The error is larger in the tropics due to stronger interferences with water vapor lines. Cloud information from the Eumetcast operational processing is used to reject observations with cloud coverage above 25%. IASI CO has been demonstrated to be a performant product in terms of sensitivity (DOFS larger than 2 in the tropics) and retrieval errors (lower than 10% in the tropics). Evaluation of IASI CO columns show discrepancies of about 7% compared to other satellite instruments [*George et al.*, 2009]. HNO_3 and CO columns for the year 2008 are used in this study.

HNO_3 observations from two other satellites, the High Resolution Dynamics Limb Sounder (HIRDLS) on the Aqua satellite and the Atmospheric Chemistry Experiment Fourier Transform Spectrometer (ACE-FTS), are used for vertical profile information. HIRDLS is a limb-scanning IR filter radiometer launched in 2004 on a near-polar Sun-synchronous orbit [*Kinnison et al.*, 2008]. The vertical resolution in the tropical upper troposphere is approximately 1 km. Individual profile precision in the retrieval is 10–15%, but comparisons indicate a low bias of up to 30% relative to ACE-FTS and MLS satellite HNO_3 observations [*Kinnison et al.*, 2008]. Observations from 2005 to 2008 are used here. ACE-FTS is a solar occultation instrument measuring infrared radiation [*Bernath et al.*, 2005]. Its orbit is optimized for high latitudes and thus provides infrequent observations in the tropics; however, complete coverage can be achieved if averaged over several years. Previous evaluation of

ACE-FTS with aircraft measurements and the GEOS-Chem model indicates a positive bias in HNO_3 of 15% in the tropical upper troposphere [*Cooper et al.*, 2011]. Observations from 2004 to 2011 are used here.

We also use aircraft data from two of NASA's Pacific Exploratory Mission campaigns to evaluate the HNO_3 simulation. The West Phase B (PEM-West B) consisted of 16 flights by the NASA DC-8 over the northwest Pacific Ocean in February–March 1994 [*Hoell et al.*, 1997]. The Tropics Phase A (PEM-Tropics A) also used the DC-8 aircraft for 17 flights throughout the tropical Pacific between New Zealand and Hawaii from August to September 1996 [*Hoell et al.*, 1999]. Individual HNO_3 measurement accuracy is reported as 30–35% [*Hoell et al.*, 1999].

Ozonesonde measurements at Kuala Lumpur (2.7°N, 101.7°E) are also used to evaluate the ozone simulation. These measurements are part of the Southern Hemisphere Additional Ozonesondes (SHADOZ) (http://croc.gsfc.nasa.gov/shadoz/) network, a group of 16 ozonesonde sites in the southern tropics [*Thompson et al.*, 2003a, 2003b]. A total of 235 ozone profiles taken from the years 1998 to 2007 are used here.

3. GEOS-Chem

The GEOS-Chem global 3-D chemical transport model [*Bey et al.*, 2001] version 9-01-03 (http://geos-chem.org) is used to interpret the IASI HNO_3 observations. GEOS-Chem is driven by assimilated meteorological data provided by the Global Modeling and Assimilation Office (GMAO) at NASA Goddard Space Flight Center. GEOS-5 meteorological fields for the year 2008 degraded to a horizontal resolution of $4° \times 5°$ are used here. The GEOS-Chem simulation has 47 vertical levels, extending from the surface to 0.1 hPa including approximately 35 levels in the troposphere. GEOS-5 employs the relaxed Arakawa-Schubert convective parameterization for shallow and deep moist convection [*Moorthi and Suarez*, 1992].

GEOS-Chem contains a detailed simulation of HO_x–NO_x–VOC-O_3-aerosol chemistry in the troposphere, including the most recent Jet Propulsion Laboratory/International Union of Pure and Applied Chemistry recommendations as implemented into GEOS-Chem by *Mao et al.* [2010]. The global lightning NO_x source of 6 Tg N a^{-1} was constrained using satellite and ozonesonde observations [*Martin et al.*, 2002, 2007] and is consistent with the 5.5 ± 2.0 Tg N a^{-1} used in current models [*Stevenson et al.*, 2013] and more recent top-down estimates from satellite observations of 6.3 ± 1.4 Tg N a^{-1} [*Miyazaki et al.*, 2014]. NO_x is distributed within simulated deep convection in a manner consistent with satellite climatologies of lightning flashes as described by *Murray et al.* [2012]. Lightning NO_x emissions are distributed relative to the cloud top height according to profiles based on aircraft observations and 3-D cloud-scale model simulations [*Ott et al.*, 2010]. Anthropogenic NO_x and CO sources are from the Emission Database for Global Atmospheric Research inventory [*Olivier*, 2001] and overwritten by regional inventories in the northern midlatitudes. Biomass burning emissions of NO_x and CO are from the Global Fire Emissions Database v3 [*van der Werf et al.*, 2010]. Biogenic CO emissions are from the Model of Gases and Aerosols from Nature (MEGAN) inventory of *Guenther et al.* [2012] as implemented by *Barkley et al.* [2011]. The mean tropical OH concentration is 1×10^6 molec/cm^3. The stratospheric ozone simulation uses the Linoz algorithm of *McLinden et al.* [2000]. Monthly mean production rates and loss frequencies for other gases in the stratosphere are computed using archived data from the Global Modeling Initiative model [*Murray et al.*, 2013]. The wet deposition scheme used in GEOS-Chem is described in *Liu et al.* [2001] with updates to subgrid scavenging by *Wang et al.* [2013]. HNO_3 is highly soluble and is often completely scavenged within the convective updraft [*Mari et al.*, 2000].

4. Interpreting IASI Tropospheric HNO_3 Columns and Results

A major challenge in inferring tropospheric HNO_3 columns from IASI observations is determining which portion of the column can be attributed to the troposphere. The coarse vertical sensitivity of IASI makes this difficult, as tropospheric HNO_3 features are smoothed in the retrieval such that they overlap into the stratosphere and vice versa.

In the comparisons that follow, GEOS-Chem (GC) profiles are smoothed using the IASI averaging kernels to simulate IASI's coarse vertical resolution. A separate averaging kernel is used for each GC grid box. This is done using the method developed by *Rodgers and Conner* [2003]:

$$\boldsymbol{x}'_{\mathrm{GC}} \approx \boldsymbol{x}_{\boldsymbol{a}} + \boldsymbol{A}(\boldsymbol{x}_{\mathrm{GC}} - \boldsymbol{x}_{\boldsymbol{a}}) \quad (1)$$

where $\boldsymbol{x}_{\mathrm{GC}}$ is the vertical HNO_3 profile from GEOS-Chem, $\boldsymbol{x}_{\boldsymbol{a}}$ is the a priori profile used in the IASI retrievals,

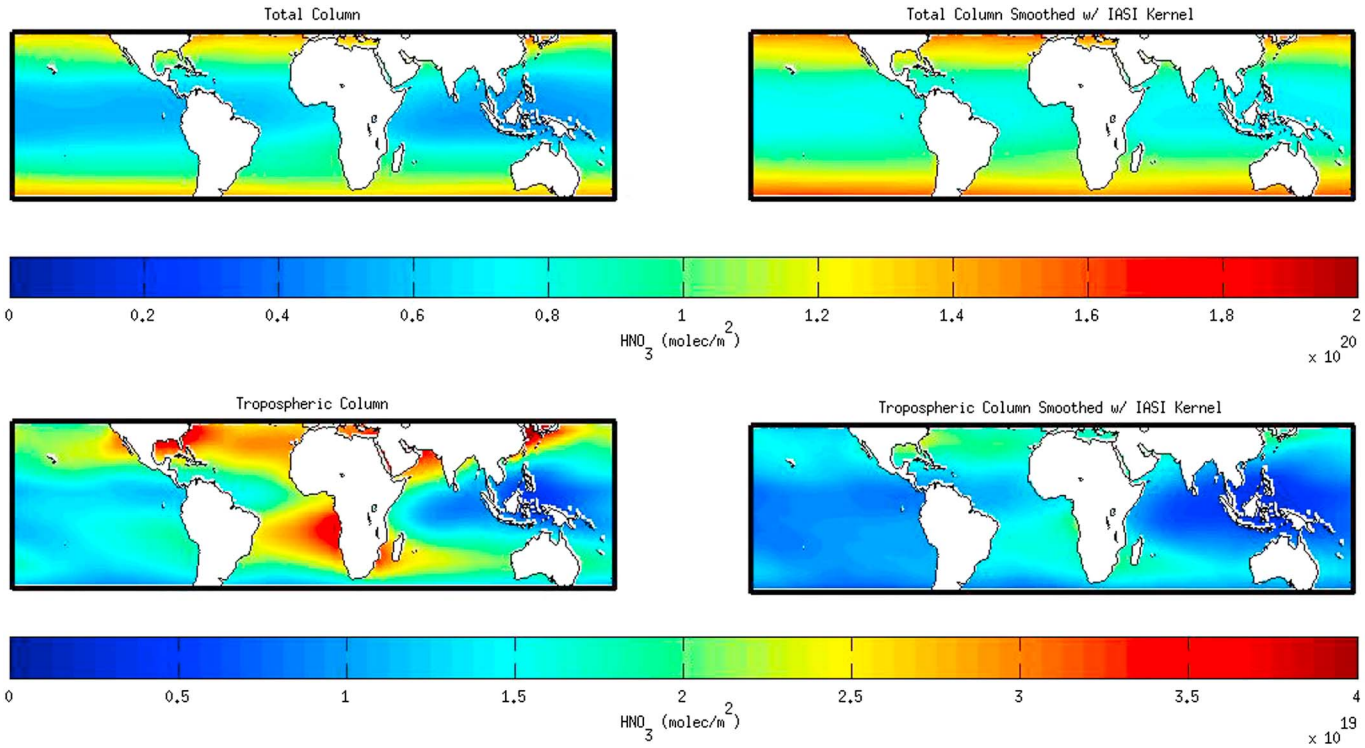

Figure 1. GEOS-Chem simulated HNO_3 columns. Subplots contain the (top) total column and total column after smoothing with IASI averaging kernels and (bottom) tropospheric column and tropospheric column after smoothing with IASI averaging kernels.

$\boldsymbol{A}$ is the IASI averaging kernel matrix, and $\boldsymbol{x}'_{GC}$ is the smoothed GEOS-Chem profile. The smoothed profile is then summed vertically to give a column value which can be compared to columns retrieved from IASI. A similar method of smoothing GEOS-Chem with remote sensing instrument averaging kernels to examine tropospheric ozone was used by *Zhang et al*. [2010].

For consistency with IASI, we first scaled the GEOS-Chem stratospheric HNO_3 production and loss rates such that the smoothed total HNO_3 column over the remote Pacific Ocean (20°S–20°N, 140°–180°W) matches the IASI column. Over the remote tropical Pacific Ocean, tropospheric HNO_3 concentrations are a small fraction (10%) of the total column abundance, and thus, the column can be treated as primarily stratospheric. Zonal symmetry in stratospheric HNO_3 concentrations then allows this scaling to be applied throughout the tropics. This results in a 25% average reduction in smoothed total simulated HNO_3 columns across the tropics.

We use GEOS-Chem to aid the separation of the stratospheric and tropospheric columns. Stratospheric columns in GEOS-Chem are calculated by setting the simulated tropospheric concentrations to zero before smoothing the simulated profiles with the IASI averaging kernels:

$$\boldsymbol{x}'_{GC\_strat} \approx \boldsymbol{x_a} + \boldsymbol{A}\left(\boldsymbol{x}_{GC(troposphere=0)} - \boldsymbol{x_a}\right) \tag{2}$$

The tropospheric columns are then calculated by subtracting the smoothed GEOS-Chem stratospheric columns from both the smoothed model total columns and the IASI total columns (Ω_{IASI}):

$$\text{Smoothed GC Trospospheric Column} = \sum_{z=0}^{\infty} \boldsymbol{x}'_{GC} - \sum_{z=0}^{\infty} \boldsymbol{x}'_{GC\_strat} \tag{3}$$

$$\text{IASI Trospospheric Column} = \Omega_{IASI} - \sum_{z=0}^{\infty} \boldsymbol{x}'_{GC\_strat} \tag{4}$$

where z is the altitude. Potential errors in the GEOS-Chem tropospheric column over the remote tropical Pacific may contribute to offset in the IASI tropospheric columns, but that offset would cancel in the difference (IASI minus GEOS-Chem) on which we focus below.

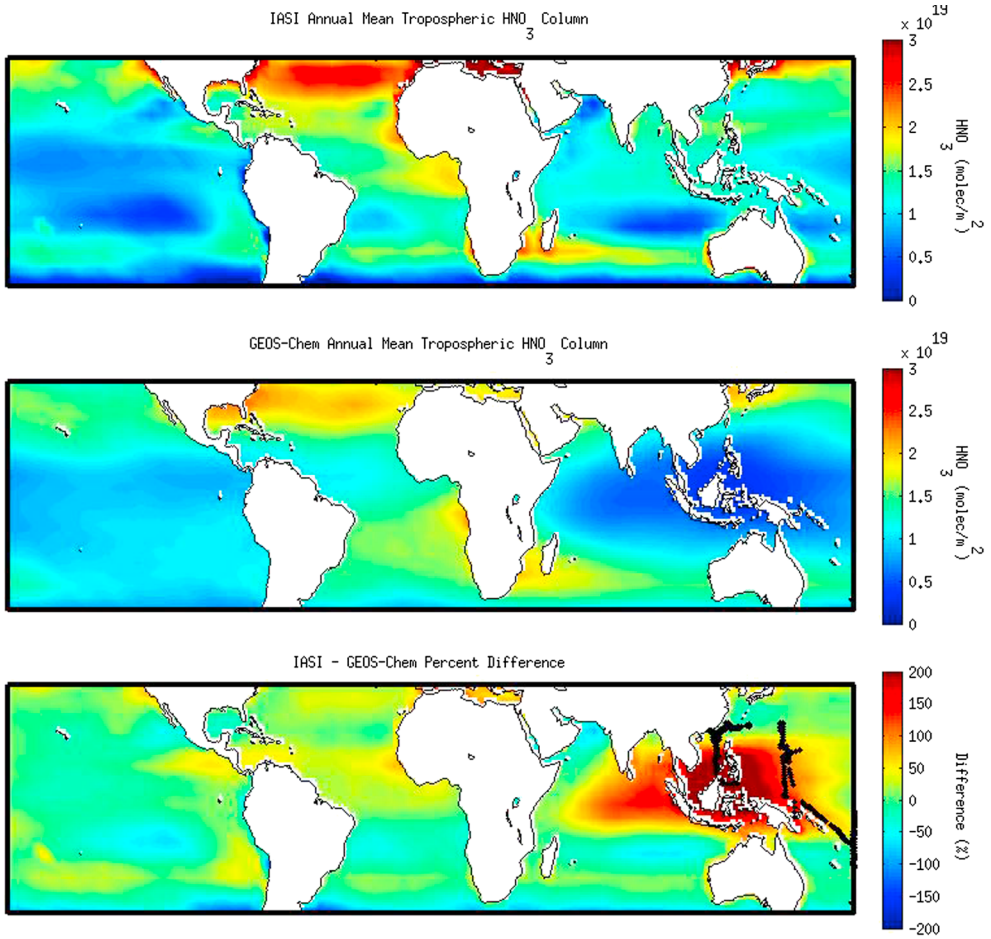

Figure 2. Annual mean tropospheric HNO_3 columns for 2008 from (top) IASI and (middle) GEOS-Chem. (bottom) The difference between IASI and GEOS-Chem. The location of PEMWest-B and PEM-Tropics A flight paths used here are shown in black in Figure 2 (bottom).

Figure 1 shows the effect of smoothing GEOS-Chem with the IASI averaging kernel. As IASI is most sensitive to the stratosphere and has coarse vertical resolution, the smoothing enhances the stratospheric component relative to the tropospheric component, leading to an apparent average reduction in the tropospheric column of 37%. This value is independent of the scaling of the stratosphere and describes a source of uncertainty in the IASI tropospheric columns due to the instrument's vertical sensitivity. Figure 1 (bottom) shows that the broad spatial patterns are retained in the smoothed tropospheric columns.

Figure 2 shows annual mean tropospheric HNO_3 columns from IASI and GEOS-Chem. Emissivity features over deserts cause overestimations in the IASI columns [*Wespes et al.*, 2009], and while this problem is largely confined to desert regions, we have ignored all observations over land as a precaution. GEOS-Chem is generally consistent with IASI over the tropics with a mean difference of 15% and a similar spatial distribution. Low concentrations over the Pacific Ocean and elevated concentrations over the tropical Atlantic are visible in both IASI and GEOS-Chem. However, IASI columns are up to twice as high as those in the simulation over the Indian Ocean and West Pacific Ocean regions (defined by 60°–160°E, 15°S–15°N, here referred to as Southeast Asia), and the Atlantic/Pacific contrast is stronger in the simulation. This bias exists throughout the year. As measurement errors in the IASI retrievals are not higher in this region than elsewhere in the tropics [*Hurtmans et al.*, 2012], the simulation is the likely source of the bias.

Figure 3 provides further evidence of a model bias through comparisons with additional satellite data. Figure 3 (column 1) shows the relative deviation from the tropical mean tropospheric HNO_3 columns near the equator (10°S–10°N) as a function of longitude for IASI and GEOS-Chem. Figure 3 (column 2) shows

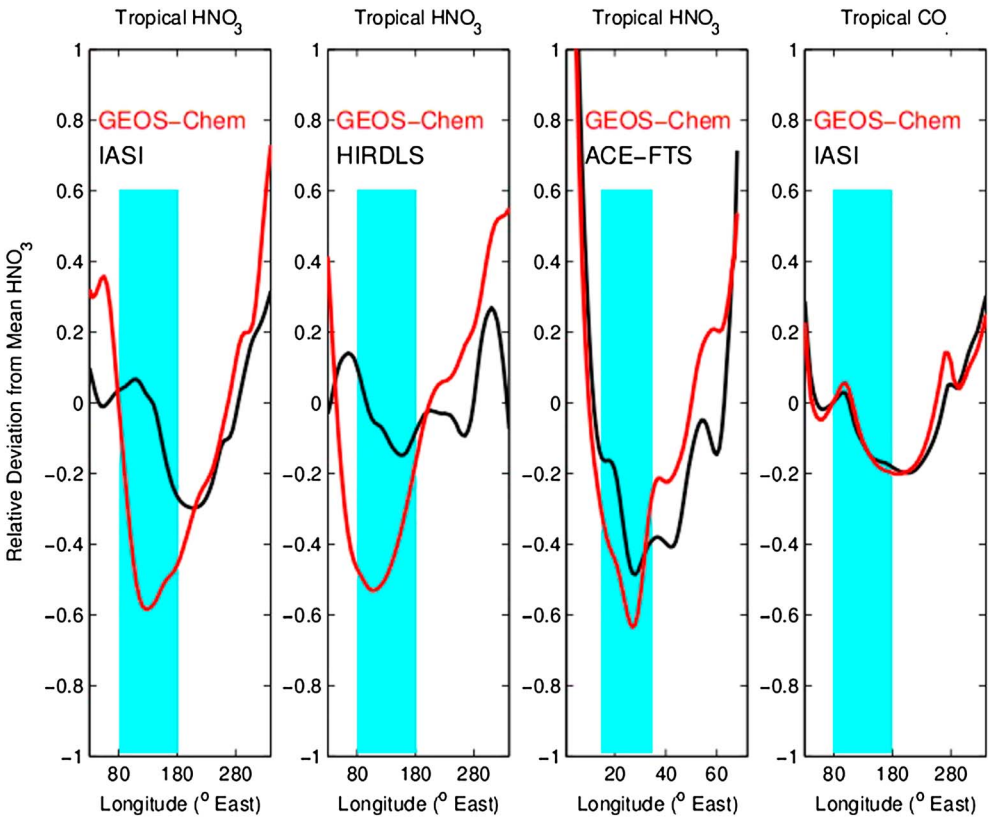

Figure 3. Relative deviation from tropical mean HNO_3 over 10°S–10°N. From left to right, (column 1) GEOS-Chem and IASI HNO_3 tropospheric columns, (column 2) GEOS-Chem and HIRDLS HNO_3 mixing ratios at 163 hPa, (column 3) GEOS-Chem and ACE-FTS HNO_3 mixing ratios at 245 hPa, and (column 4) GEOS-Chem and IASI CO total columns. Figure 3 (columns 1–3) shows an underestimation in GEOS-Chem HNO_3 over Southeast Asia (shaded region spanning longitudes 80°–180°). Figure 3 (column 4) shows no bias over Southeast Asia.

this deviation calculated from the HIRDLS HNO_3 concentration at 163 hPa. Figure 3 (column 3) uses ACE-FTS HNO_3 concentrations near 245 hPa. GEOS-Chem is sampled at the location and day of observations for each instrument. Since IASI gives column values and ACE-FTS and HIRDLS provide upper tropospheric concentrations, all three plots are normalized by their tropical mean values to facilitate comparisons, as well as to reduce the effect of instrument biases. All three plots show the familiar wave-one pattern of elevated concentrations over the tropical Atlantic (longitude range 0°–20° and 310°–360°). IASI shows a small local maximum over the Southeast Asia region (longitudes 60°–160°E) that is more pronounced than that seen in the plots for ACE-FTS or HIRDLS. Differences between instruments likely reflect different vertical layers of observation (column versus upper troposphere) and sampling differences in this cloudy region. However, all three plots also show that GEOS-Chem underestimates HNO_3 over this region. The ACE-FTS plot is consistent with previous evaluations of GEOS-Chem by *Cooper et al.* [2011], which showed that GEOS-Chem underestimates NO_y concentrations relative to MOZAIC and HNO_3 relative to ACE-FTS in the region.

Figure 4 shows vertical HNO_3 profiles from measurements made in the Southeast Asia region only during the PEM-West B and PEM-Tropics A aircraft campaigns and from GEOS-Chem. The simulation is run using GMAO MERRA reanalysis meteorological fields for the campaign years (1994 for PEM-West B and 1996 for PEM-Tropics A) and is sampled along the aircraft flight path at the same location, altitude, and time of the observations. The simulation is consistently lower than the aircraft measurements by a factor of 2–3 throughout the middle and upper troposphere. This supports the bias in the simulation, as this is a consistent feature over a large vertical and horizontal range observed independently by satellite and aircraft measurements.

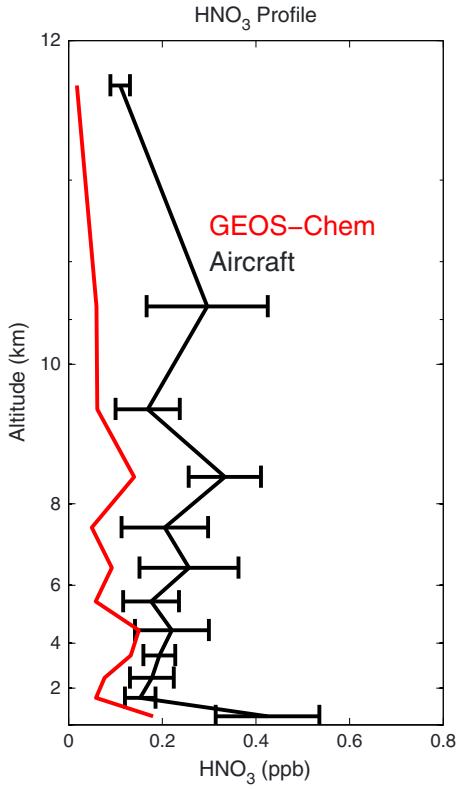

Figure 4. Average HNO_3 profiles from aircraft campaigns (PEM-West B and PEM-Tropics A) and from GEOS-Chem sampled along the flight paths. Error bars indicate 1 standard error from the mean.

5. Understanding the GEOS-Chem Bias

In the following sections we examine the most likely sources of the model underestimate in Southeast Asia: transport errors, the lightning NO_x source and its subsequent chemical processes, and overly vigorous wet deposition.

5.1. Mixing Processes

CO measurements are useful in model evaluation as combustion NO_x sources are collocated with CO emissions, and the lifetime of CO is sufficiently long to evaluate transport [*Jaeglé et al.*, 1998]. Figure 3 (column 4) shows the relative deviation from the tropical mean CO total columns for GEOS-Chem and IASI. The deviation from the mean in the GEOS-Chem simulation agrees well with IASI throughout the tropics, including the Southeast Asia region where the bias in HNO_3 exists. The absence of errors in CO indicates that transport from combustion sources is an unlikely contributor to the HNO_3 bias. We next turn to lightning NO_x as a potential contributor to the HNO_3 bias that is independent of CO.

5.2. Lightning NO_x Yield per Flash

We first examine the magnitude of the lightning NO_x source over Southeast Asia. In the year 2008 the standard GEOS-Chem simulation has a lightning NO_x source of 6.2 Tg N a^{-1}. Figure 5 shows the effect of adding additional lightning NO_x to the free troposphere. A factor of 3.5 increase in lightning NO_x yield/flash over Southeast Asia yields a 2.4 Tg N a^{-1} increase in the total global annual mean lightning NO_x source to 8.6 Tg N a^{-1}. The GEOS-Chem HNO_3 column bias versus IASI over the Indian Ocean and Indonesia is reduced from 92% to 7%. Agreement is also improved over the West Pacific. Figure 6 evaluates the implications for the O_3 simulation at Kuala Lumpur. The additional NO_x leads to increased ozone production which causes errors of 25% in the simulated ozone fields. This indicates that a simple increase in the lightning NO_x source is not the ideal solution to the simulated column HNO_3 underestimate.

5.3. Vertical Distribution of Lightning NO_x

The effects of lightning NO_x on tropospheric chemistry depend on its vertical distribution, as NO_x lifetimes and ozone production efficiencies generally increase with altitude [*Labrador et al.*, 2005]. The profiles developed by *Ott et al.* [2010] used to distribute lightning NO_x emissions vertically are based on information from midlatitude and subtropical storms and might not be representative of tropical storms. We performed sensitivity studies by increasing the median injection height of tropical lightning NO emissions from 8.7 to 12.6 km. We find that raising the NO injection height increases the HNO_3 tropospheric column abundances throughout the tropics by as much as 25% but has little effect in the regions where lightning NO is emitted as shown in Figure 5c. NO_x emitted at higher altitude has a longer lifetime and can be transported horizontally to form HNO_3 away from the source region. This HNO_3 also has a longer lifetime at these altitudes leading to the increased column abundances throughout the tropics. However, near the region of emission the increase in HNO_3 produced at higher altitudes is largely balanced by decreases at lower altitudes and does not significantly change the column abundance. Thus, adjustments to the NO_x injection height do not improve the simulation bias in Southeast Asia. The resulting change in ozone concentrations throughout the tropics is generally less than a few parts per billion as shown in Figure 6.

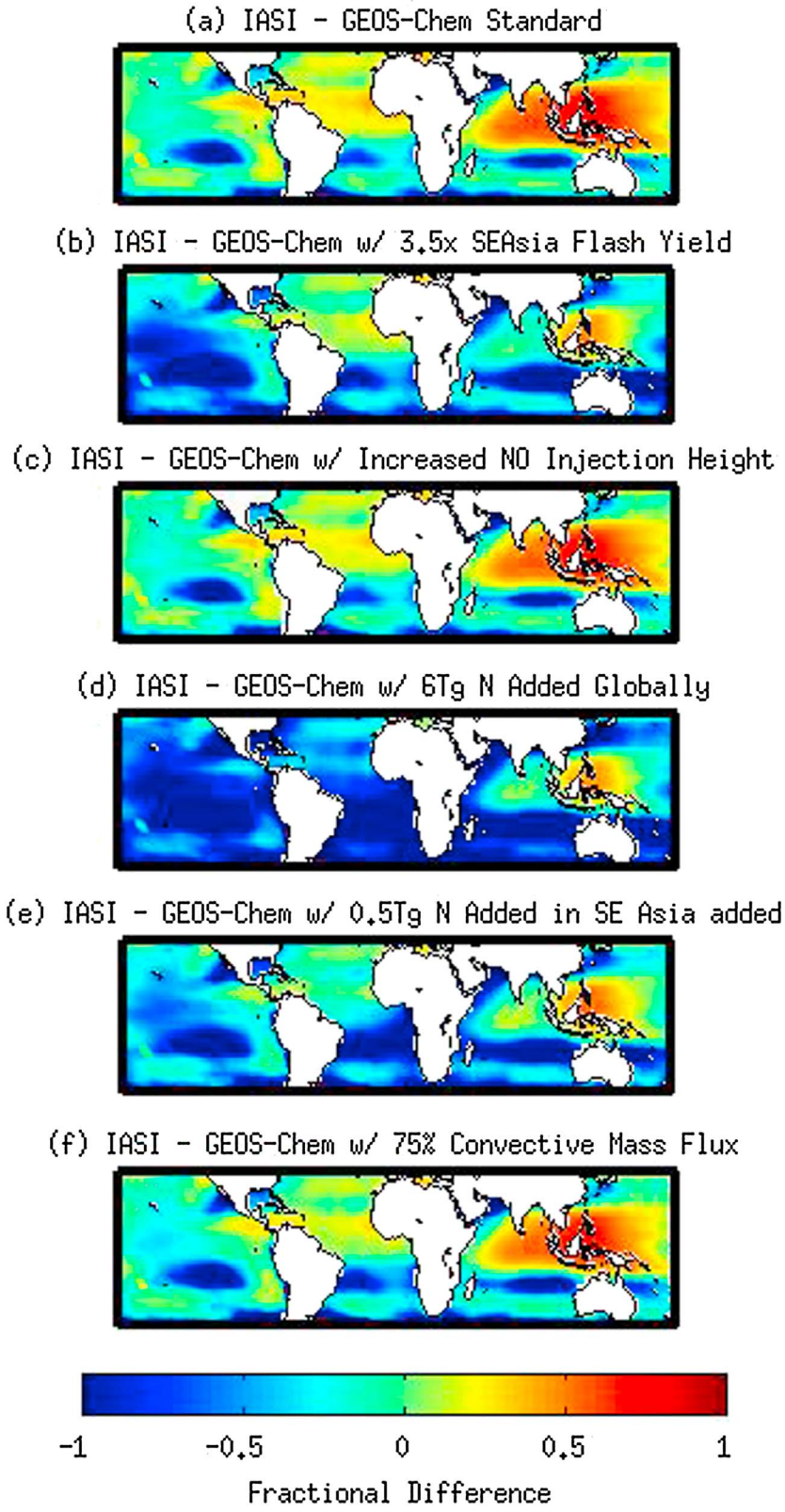

Figure 5. Fractional difference in annual mean tropospheric HNO_3 columns between IASI and the following GEOS-Chem simulations: (a) standard simulation, (b) with flash yield increased by factor of 3.5 (c) with median NO injection height increased from 8.7 to 12.6 km, (d) with 6 Tg additional HNO_3 globally, (e) with 0.5 Tg additional HNO_3 over Southeast Asia only, and (f) with convective mass fluxes reduced by 25%.

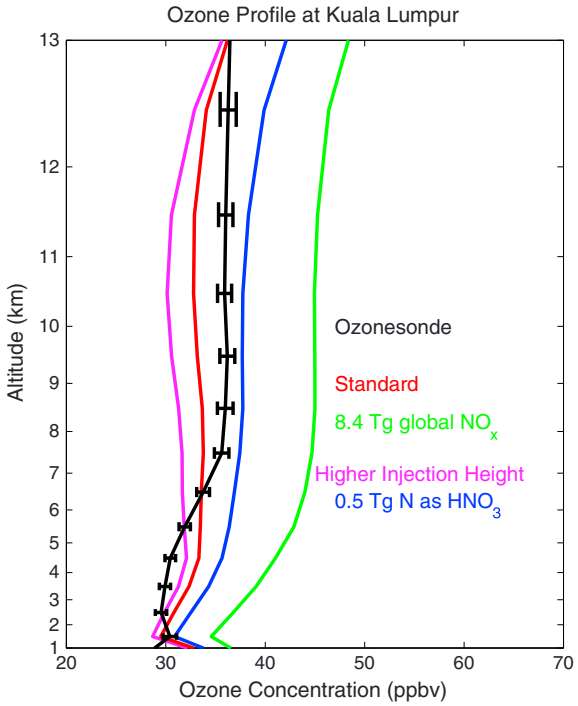

Figure 6. Annual mean ozone profile at Kuala Lumpur (2.7°N, 101.7°E). Profiles from a standard GEOS-Chem simulation (red), a simulation with 0.5 Tg HNO_3 added in Southeast Asia (blue), a simulation with the lightning NO source increased to 8.4 Tg (green), a simulation with lightning NO injection height raised to 12.6 km (pink), and an annual mean profile from ozonesondes (black) are shown. Error bars represent the standard error in the ozonesonde measurements.

5.4. Subgrid Plume Parameterization

The method by which lightning NO_x is emitted in the simulation may contribute to the simulation bias. Lightning NO_x emitted into the GEOS-Chem grid boxes produce dilute NO plumes with typical concentrations less than 1 ppbv. Aircraft observations found that lightning can create highly concentrated NO plumes inside cumulonimbus clouds, with concentrations generally between 1 and 7 ppbv and occasionally rising as high as 25 ppbv [*Huntrieser et al.*, 2002, 2009; *Ott et al.*, 2010]. These concentrated plumes can have spatial scales as small as 300 m [*Huntrieser et al.*, 2002], which are not resolved in global models with typical scales of 50–500 km. Ozone production from lightning NO_x is highly nonlinear with respect to NO_x concentration [*Lin et al.*, 1988]. As a result, the dilute NO_x plumes created in GEOS-Chem overestimate the ozone production efficiency (OPE), or the number of ozone molecules produced per NO_x molecule consumed. This means that O_3 is produced too efficiently and HNO_3 is produced too inefficiently. Similar issues have been noted in the representation of plumes from power plants [*Sillman et al.*, 1990], aircraft [*Meijer et al.*, 1997], and ships [*Vinken et al.*, 2011]. Changes to the lightning NO_x parameterization which account for this nonlinearity may reduce the simulated HNO_3 bias over Southeast Asia.

We explored this process by modifying the GEOS-Chem lightning simulation to account for the nonlinear chemistry that occurs in the early concentrated stage of a lightning NO_x plume before it dilutes to grid box scale. This is done by allowing some of the lightning NO to rapidly convert to HNO_3 after a typical amount of ozone production. The ratio of O_3 to HNO_3 produced is treated as a constant OPE of 15 moles of O_3 per mole of HNO_3. This value was estimated by forcing NO_x concentrations in a GEOS-Chem grid box over Indonesia to 5 ppbv (near the middle of the measured 1–7 ppbv range for lightning plumes), calculating the instantaneous OPE and finding an average of 15 moles O_3/mole NO. This value is similar to those found by modeling studies for urban pollution (5–20 mol/mol) [*Kleinman et al.*, 2002] and for aircraft NO_x emissions (10–28 mol/mol) [*Gilmore et al.*, 2013].

Figure 5d shows the change in HNO_3 from adding globally 6 Tg N yr^{-1} with an OPE of 15 mol/mol. The lightning NO source was held fixed at 6 Tg N a^{-1}, while the amount of extra N (emitted as HNO_3) and O_3 was allowed to vary given uncertainty in plume dilution rates. The bias over Southeast Asia is reduced from 92% to 9% but at the expense of increasing the bias throughout the rest of the tropics to −46%.

It is possible that lightning plumes over Southeast Asia have different behavior than elsewhere as lightning NO_x yields are known to vary by region [*Schumann and Huntrieser*, 2007]. With this in mind, 0.5 Tg N is added with an OPE of 15 mol/mol over Southeast Asia only in Figure 5e. The bias over Southeast Asia is reduced to 6% without negatively affecting the rest of the tropics. Figure 6 evaluates how the additional O_3 (30 Tg) from this parameterization affects the O_3 simulation. Free tropospheric ozone concentrations in Southeast Asia increased by up to 7 ppbv (up to a 17% increase) with small increases elsewhere. Ozone in the middle troposphere remains within 25% of ozonesondes at Kuala Lumpur. The processes affecting lightning NO_x over Southeast Asia differently than the rest of the globe is not fully

understood at this time. Satellite observations show that lightning flashes in this region have higher radiances and have a larger spatial footprint than elsewhere in the tropics [*Beirle et al*., 2014]. Also, intracloud lightning flashes, which dissipate more energy, occur more frequently in this region [*Cooray*, 1997; *Mackerras et al*., 1998]. Lightning in GEOS-Chem is scaled by flash count and uses a single value for LNO_x produced per flash count in the tropics. Such parameterizations do not account for regional differences in flash radiance or length, or distinguish between intracloud and cloud-to-ground lightning and are thus likely affected by regional biases.

5.5. Convection and Wet Deposition

The effects of convective activity on HNO_3 may play a role in the observed bias as Southeast Asia is a highly active convection region. *Staudt et al*. [2003] found that simulated HNO_3 concentrations are sensitive to the convective mass flux due to both scavenging of HNO_3 in updrafts and mixing of air in the boundary layer where it can be deposited. We explored the potential effect that convection has on modeled HNO_3 by decreasing the convective mass flux by 25%. Figure 5f shows that this change in convective flux has little effect on the bias with respect to IASI tropospheric columns, increasing columns over the tropics by less than 15%. We also tested the effect of wet deposition alone, by reducing the scavenging efficiency in GEOS-Chem. A 50% reduction in the scavenging efficiency leads to a 10% increase in tropospheric HNO_3 columns. The reduction in solubility tested here is not physically likely, but these tests indicate that the convective scavenging scheme or errors in parameterized convection may play a role in the HNO_3 bias, although the overall sensitivity of the bias to scavenging is small compared to changes in lightning NO_x.

6. Conclusions

We analyzed IASI tropospheric HNO_3 columns over the tropical ocean. IASI and GEOS-Chem tropospheric HNO_3 columns are consistent within 10% throughout most of the tropics. However, observations over Southeast Asia show column values twice as high as simulated values. This simulated HNO_3 bias was supported by aircraft measurements (PEM-West B and PEM-Tropics A) and observations from the ACE-FTS and HIRDLS satellite instruments. Comparison of IASI and GEOS-Chem CO did not indicate a bias, implying large-scale transport errors are an unlikely explanation for the HNO_3 bias.

Investigation into the source of the model bias indicates sensitivity to the lightning NO_x parameterization. We found that direct changes to the lightning NO_x source was unlikely to explain the bias as a large (factor of 3.5) increase was needed, which in turn led to a 25% bias in simulated ozone concentrations relative to ozonesonde observations. Studies examining the sensitivity of tropospheric HNO_3 columns to the vertical distribution of lightning NO_x emissions indicated that increasing the NO_x injection height had little effect on the simulation bias, although it led to increased column abundances by 25% away from the region of emission. A simple parameterization accounting for nonlinearities in the conversion of NO_x to HNO_3 in the beginning stage of the lightning NO_x plume and the related ozone production chemistry was implemented with moderate success. A prescribed subgrid ozone production efficiency of 15 mol/mol in conjunction with an additional 0.5 Tg N added over Southeast Asia reduced the bias in that region from 92% to 6% with minimal impact on simulated ozone concentrations.

We also found some sensitivity of the model bias to convection processes, both in convective mass flux and the HNO_3 wet deposition parameterization. Improved agreement between IASI and GEOS-Chem in convectively active regions was achieved by either reducing the convective mass flux or the efficiency of wet scavenging in convective although the overall effects were small. The most likely solution to the model bias will include changes to multiple processes, although changes to lightning NO_x may have a greater effect.

Future work should consider a more sophisticated lightning plume model in which the OPE depends on local dilution rates, perhaps similar to the parameterization for ship emissions [*Vinken et al*., 2011]. Additional processes not tested here, including errors in HNO_3 production from NO_2, HNO_3 photolysis in clouds, PAN chemistry, or uptake of HNO_3 by ice crystals [*von Kuhlmann and Lawrence*, 2006] may play a role. The recent development of a stratospheric HNO_3 simulation for GEOS-Chem by *Eastham et al*. [2014] will aid future efforts to separate stratospheric and tropospheric components from the IASI total columns.

Acknowledgments

IASI HNO_3 data are available on request by contacting P.-F Coheur. IASI CO data were provided by LATMOS/CNRS and ULB and are available online at the Ether database at http://www.pole-ether.fr/. HIRDLS data products are available online at NASA's Goddard Earth Sciences Data and Information Services Center. ACE-FTS data are available on request by contacting the ACE Science Team at info@scisat.ca. Aircraft data from PEM West and PEM-Tropics campaigns are made available online at NASA's Global Tropospheric Experiment webpage at http://www-gte.larc.nasa.gov/gte_fld.htm. SHADOZ ozonesonde measurements are available online at http://croc.gsfc.nasa.gov/shadoz/. Information on accessing GEOS-Chem code can be found online at geos-chem.org. This work was supported by the Natural Sciences and Engineering Research Council of Canada. P.-F. Coheur and C. Wespes are, respectively, Senior Research Associate and Postdoctoral Researcher with F.R.S.-FNRS. The research in Belgium was also funded by the Belgian State Federal Office for Scientific, Technical and Cultural Affairs and the European Space Agency (ESA Prodex IASI.Flow), as well as by EUMETSAT (O3MSAF).

References

Barkley, M. P., et al. (2011), Can a "state of the art" chemistry transport model simulate Amazonian tropospheric chemistry?, *J. Geophys. Res.*, *116*, D16302, doi:10.1029/2011JD015893.

Beirle, S., W. Koshak, R. Blakeslee, and T. Wagner (2014), Global patterns of lightning properties derived by OTD and LIS, *Nat. Hazards Earth Syst. Sci. Discuss.*, *2*, 2765–2787, doi:10.5194/nhessd-2-2765-2014.

Bernath, P. F., et al. (2005), Atmospheric Chemistry Experiment (ACE): Mission overview, *Geophys. Res. Lett.*, *32*, L15S01, doi:10.1029/2005GL022386.

Bey, I., D. J. Jacob, R. M. Yantosca, J. A. Logan, B. Field, A. M. Fiore, Q. Li, H. Liu, L. J. Mickley, and M. Schultz (2001), Global modeling of tropospheric chemistry with assimilated meteorology: Model description and evaluation, *J. Geophys. Res.*, *106*, 23,073–23,096, doi:10.1029/2001JD000807.

Brunner, D., et al. (2005), An evaluation of the performance of chemistry transport models—Part 2: Detailed comparison with two selected campaigns, *Atmos. Chem. Phys.*, *5*, 107–129, doi:10.5194/acp-5-107-2005.

Clerbaux, C., et al. (2009), Monitoring of atmospheric composition using the thermal infrared IASI/MetOp sounder, *Atmos. Chem. Phys.*, *9*, 6041–6054.

Cooper, M., R. V. Martin, B. Sauvage, C. D. Boone, K. A. Walker, P. F. Bernath, C. A. McLinden, D. A. Degenstein, A. Volz-Thomas, and C. Wespes (2011), Evaluation of ACE-FTS and OSIRIS satellite retrievals of ozone and nitric acid in the tropical upper troposphere: Application to ozone production efficiency, *J. Geophys. Res.*, *116*, D12306, doi:10.1029/2010JD015056.

Cooray, V. (1997), Energy dissipation in lightning flashes, *J. Geophys. Res.*, *102*(D17), 21,401–21,410, doi:10.1029/96JD01917.

Eastham, S. D., D. K. Weisenstein, and S. R. H. Barrett (2014), Development and evaluation of the unified tropospheric-stratospheric chemistry extension (UCX) for the global chemistry-transport model GEOS-Chem, *Atmos. Environ.*, *89*, 52–63, doi:10.1016/j.atmosenv.2014.02.001.

Folkins, I., P. Bernath, C. Boone, L. J. Donner, A. Eldering, G. Lesins, R. V. Martin, B.-M. Sinnhuber, and K. Walker (2006), Testing convective parameterizations with tropical measurements of HNO_3, CO, H_2O, and O_3: Implications for the water vapor budget, *J. Geophys. Res. 111*, D23304, doi:10.1029/2006JD007325.

George, M., et al. (2009), Carbon monoxide distributions from the IASI/METOP mission: Evaluation with other space-borne remote sensors, *Atmos. Chem. Phys.*, *9*, 8317–8330, doi:10.5194/acp-9-8317-2009.

Gille, J. C., et al (1984), Accuracy and precision of the nitric acid concentration determined by the Limb Infrared Monitor of the Stratosphere experiment on the Nimbus 7, *J. Geophys. Res.*, *89*, 5179–5190, doi:10.1029/JD089iD04p05179.

Gilmore, C. K., S. R. H. Barrett, J. Koo, and Q. Wang (2013), Temporal and spatial variability in the aviation NO_x-related O_3 impact, *Environ. Res. Lett.*, *8*, 034,027, doi:10.1088/1748-9326/8/3/034027.

Giorgi, F., and W. L. Chameides (1986), Rainout lifetimes of highly soluble aerosols and gases as inferred from simulations with a general-circulation model, *J. Geophys. Res.*, *91*, 14,367–14,376, doi:10.1029/JD091iD13p14367.

Guenther, A. B., X. Jiang, C. L. Heald, T. Sakulyanontvittaya, T. Duhl, L. K. Emmons, and X. Wang (2012), The Model of Emissions of Gases and Aerosols from Nature version 2.1 (MEGAN2.1): An extended and updated framework for modeling biogenic emissions, *Geosci. Model Dev. Discuss.*, *5*, 1503–1560, doi:10.5194/gmdd-5-1503-2012.

Hoell, J. M., D. D. Davis, S. C. Liu, R. E. Newell, H. Akimoto, R. J. McNeal, and R. J. Bendura (1997), The Pacific Exploratory Mission-West Phase B: February–March, 1994, *J. Geophys. Res.*, *102*(D23), 28,223–28,239, doi:10.1029/97JD02581.

Hoell, J. M., D. D. Davis, D. J. Jacob, M. O. Rodgers, R. E. Newell, H. E. Fuelberg, R. J. McNeal, J. L. Raper, and R. J. Bendura (1999), Pacific Exploratory Mission in the tropical Pacific: PEM-Tropics A, August–September 1996, *J. Geophys. Res.*, *104*(D5), 5567–5583, doi:10.1029/1998JD100074.

Huntrieser, H., et al. (2002), Airborne measurements of NO_x, tracer species, and small particles during the European Lightning Nitrogen Oxides Experiment, *J. Geophys. Res.*, *107*(D11), 4113, doi:10.1029/2000JD000209.

Huntrieser, H., et al. (2009), NO_x production by lightning in Hector: First airborne measurements during SCOUT-O3/ACTIVE, *Atmos. Chem. Phys.*, *9*, 8377–8412, doi:10.5194/acp-9-8377-2009.

Hurtmans, D., P.-F. Coheur, C. Wespes, L. Clarisse, O. Scharf, C. Clerbaux, J. Hadji-Lazaro, M. George, and S. Turquety (2012), FORLI radiative transfer and retrieval code for IASI, *J. Quant. Spectros. Radiat. Transf.*, *113*(11), 1391–1408.

Jaeglé, J., D. J. Jacob, Y. Wang, A. J. Weinheimer, B. A. Ridley, T. L. Campos, G. W. Sachse, and D. E. Hagen (1998), Sources and chemistry of NO_x in the upper troposphere over the United States, *Geophys. Res. Lett.*, *25*(10), 1705–1708, doi:10.1029/97GL03591.

Kasibhatla, P. S., H. Levey II, and W. J. Moxim (1993), Global NO_x, HNO_3, PAN, and NO_y distributions from fossil fuel combustion emissions: A model study, *J. Geophys. Res.*, *98*(D4), 7165–7180, doi:10.1029/92JD02845.

Kinnison, D. E., et al. (2008), Global observations of HNO_3 from the High Resolution Dynamics Limb Sounder (HIRDLS): First results, *J. Geophys. Res.*, *113*, D16S44, doi:10.1029/2007JD008814.

Kleinman, L. I., P. H. Daum, Y.-N. Lee, L. J. Nunnermacker, S. R. Springston, J. Weinstein-Lloyd, and J. Rudolph (2002), Ozone production efficiency in an urban area, *J. Geophys. Res.*, *107*(D23), 4733, doi:10.1029/2002JD002529.

Koshak, W. J., H. Peterson, A. Biazar, M. Khan, and L. Wang (2013), The NASA Lightning Nitrogen Oxides Model (LNOM): Application to air quality modeling, *Atmos. Res.*, doi:10.1016/j.atmosres.2012.12.015.

Labrador, L. J., R. von Kuhlmann, and M. G. Lawrence (2005), The effects of lightning-produced NO_x and its vertical distribution on atmospheric chemistry: Sensitivity simulations with MATCH-MPIC, *Atmos. Chem. Phys.*, *5*, 1815–1834, doi:10.5194/acp-5-1815-2005.

Lin, X., M. Trainer, and S. C. Liu (1988), On the nonlinearity of the tropospheric ozone production (1988), *J. Geophys. Res.*, *93*(D12), 15,879–15,888, doi:10.1029/JD093iD12p15879.

Liu, H., D. J. Jacob, I. Bey, and R. M. Yantosca (2001), Constraints from ^{210}Pb and ^{7}Be on wet deposition and transport in a global three-dimensional chemical tracer model driven by assimilated meteorological fields, *J. Geophys. Res.*, *101*(D11), 12,109–12,128, doi:10.1029/2000JD900839.

Liu, S. C., M. Trainer, F. C. Fehsenfeld, D. D. Parrish, E. J. Williams, D. W. Fahey, G. Huebler, and P. C. Murphy (1987), Ozone production in the rural troposphere and the implications for regional and global ozone distributions, *J. Geophys. Res.*, *92*, 4191–4207, doi:10.1029/JD092iD04p04191.

Mackerras, D., M. Darveniza, R. E. Orville, E. R. Williams, and S. J. Goodman (1998), Global lightning: Total, cloud and ground flash estimates, *J. Geophys. Res.*, *103*(D16), 19,791–19,809, doi:10.1029/98JD01461.

Mao, J., et al. (2010), Chemistry of hydrogen oxide radicals (HO_x) in the Arctic troposphere in spring, *Atmos. Chem. Phys.*, *10*(13), 5823–5838, doi:10.5194/acp-10-5823-2010.

Mari, C., D. J. Jacob, and P. Bechtold (2000), Transport and scavenging of soluble gases in a deep convective cloud, *J. Geophys. Res.*, *105*(D17), 22,255–22,267, doi:10.1029/2000JD900211.

Martin, R. V., et al. (2002), Interpretation of TOMS observations of tropical tropospheric ozone with a global model and in situ observations, *J. Geophys. Res.*, *107*(D18), 4351, doi:10.1029/2001JD001480.

Martin, R. V., B. Sauvage, I. Folkins, C. E. Sioris, C. Boone, P. Bernath, and J. R. Ziemke (2007), Space-based constraints on the production of nitric oxide by lightning, *J. Geophys. Res.*, *112*, D09309, doi:10.1029/2006JD007831.

McLinden, C. A., S. C. Olsen, B. Hannegan, O. Wild, M. J. Prather, and J. Sundet (2000), Stratospheric ozone in 3-D models: A simple chemistry and the cross-tropopause flux, *J. Geophys. Res.*, *105*(D11), 14,653–14,665, doi:10.1029/2000JD900124.

Meijer, E. W., P. F. J. van Velthoven, W. M. F. Wauben, J. P. Beck, and G. J. M. Velders (1997), The effects of the conversion of nitrogen oxides in aircraft exhaust plumes in global models, *Geophys. Res. Lett.*, *24*(23), 3013–3016, doi:10.1029/97GL53156.

Miyazaki, K., H. J. Eskes, K. Sudo, and C. Zhang (2014), Global lightning NO_x production estimated by an assimilation of multiple satellite data sets, *Atmos. Chem. Phys.*, *14*, 3277–3305, doi:10.5194/acp-14-3277-2014.

Moorthi, S., and M. J. Suarez (1992), Relaxed Arakawa-Schubert, a parameterization of moist convection for general circulation models, *Mon. Weather Rev.*, *120*, 978–1002.

Murray, L. T., D. J. Jacob, J. A. Logan, R. C. Hudman, and W. J. Koshak (2012), Optimized regional and interannual variability of lightning in a global chemical transport model constrained by LIS/OTD satellite data, *J. Geophys. Res.*, *117*, D20307, doi:10.1029/2012JD017934.

Murray, L. T., J. A. Logan, and D. J. Jacob (2013), Interannual variability in tropical tropospheric ozone and OH: The role of lightning, *J. Geophys. Res. Atmos.*, *118*, 11,468–11,480, doi:10.1002/jgrd.50857.

Olivier, J. G. (2001), *Global Emissions Sources and Sinks*, The Climate System, A.A. Balkema Publishers/Sweets & Zeitlinger Publishers, Lisse, Netherlands.

Ott, L. E., K. E. Pickering, G. L. Stenchikov, D. J. Allen, A. J. DeCaria, B. Ridley, R.-F. Lin, S. Lang, and W.-K. Tao (2010), Production of lightning NO_x and its vertical distribution calculated from three-dimensional cloud-scale chemical transport model simulations, *J. Geophys. Res.*, *115*, D04301, doi:10.1029/2009JD011880.

Pickering, K. E., A. M. Thompson, R. R. Dickerson, W. T. Luke, D. P. McNamara, J. P. Greenberg, and P. R. Zimmerman (1990), Model calculations of tropospheric ozone production potential following observed convective events, *J. Geophys. Res.*, *95*(D9), 14,049–14,062, doi:10.1029/JD095iD09p14049.

Rodgers, C. D., and B. J. Conner (2003), Intercomparison of remote sounding instruments, *J. Geophys. Res.*, *108*(D3), 4116, doi:10.1029/2002JD002299.

Santee, M. L., G. L. Manney, N. J. Livesey, and W. G. Read (2004), Three-dimensional structure and evolution of stratospheric HNO_3 based on UARS Microwave Limb Sounder measurements, *J. Geophys. Res.*, *109*, D15306, doi:10.1029/2004JD004578.

Sauvage, B., R. V. Martin, A. van Donkelaar, and J. R. Ziemke (2007), Quantification of the factors controlling tropical tropospheric ozone and the South Atlantic maximum, *J. Geophys. Res.*, *112*, D11309, doi:10.1029/2006JD008008.

Schumann, U., and H. Huntrieser (2007), The global lightning-induced nitrogen oxides source, *Atmos. Chem. Phys.*, *7*, 3823–3907, doi:10.5194/acp-7-3823-2007.

Sillman, S., J. A. Logan, and S. C. Wofsy (1990), A regional scale model for ozone in the United States with subgrid representation of urban and power plant plumes, *J. Geophys. Res.*, *95*(D5), 5731–5748, doi:10.1029/JD095iD05p05731.

Singh, H. B., et al. (2007), Reactive nitrogen distribution and partitioning in the North American troposphere and lowermost stratosphere, *J. Geophys. Res.*, *112*, D12S04, doi:10.1029/2006JD007664.

Staudt, A. C., D. J. Jacob, F. Ravetta, J. A. Logan, D. Bachiochi, T. N. Krishnamurti, S. Sandholm, B. Ridley, H. B. Singh, and B. Talbot (2003), Sources and chemistry of nitrogen oxides over the tropical Pacific, *J. Geophys. Res.*, *108*(D2), 8239, doi:10.1029/2002JD002139.

Stevenson, D. S., et al. (2013), Tropospheric ozone changes, radiative forcing and attribution to emissions in the Atmospheric Chemistry and Climate Model Intercomparison Project (ACCMIP), *Atmos. Chem. Phys.*, *13*, 3063–3085, doi:10.5194/acp-13-3063-2013.

Thompson, A. M., et al. (2003a), Southern Hemisphere Additional Ozonesondes (SHADOZ) 1998–2000 tropical ozone climatology: 1. Comparison with Total Ozone Mapping Spectrometer (TOMS) and ground-based measurements, *J. Geophys. Res.*, *108*(D2), 8238, doi:10.1029/2001JD000967.

Thompson, A. M., et al. (2003b), Southern Hemisphere Additional Ozonesondes (SHADOZ) 1998–2000 tropical ozone climatology: 2. Tropospheric variability and the zonal wave-one, *J. Geophys. Res.*, *108*(D2), 8241, doi:10.1029/2002JD002241.

Tost, H., P. J. Joeckel, and J. Lelieveld (2007), Lightning and convection parameterisations—Uncertainties in global modelling, *Atmos. Chem. Phys.*, *7*(17), 4553–4568.

Tsidu, G. M., et al. (2005), NO_y from Michelson Interferometer for passive atmospheric sounding on environmental satellite during the Southern Hemisphere polar vortex split in September/October 2002, *J. Geophys. Res.*, *110*, D11301, doi:10.1029/2004JD005322.

van der Werf, G. R., J. T. Randerson, L. Giglio, G. J. Collatz, M. Mu, P. S. Kasibhatla, D. C. Morton, R. S. DeFries, Y. Jin, and T. T. van Leeuwen (2010), Global fire emissions and the contribution of deforestation, savanna, forest, agricultural, and peat fires (1997–2009), *Atmos. Chem. Phys.*, *10*, 11,707–11,735, doi:10.5194/acp-10-11707-2010.

Vinken, G. C., K. F. Boersma, D. J. Jacob, and E. W. Meijer (2011), Accounting for non-linear chemistry of ship plumes in the GEOS-Chem global chemistry transport model, *Atmos. Chem. Phys.*, *11*, 11,707–11,722, doi:10.5194/acp-11-11707-2011.

Von Kuhlmann, R., and M. G. Lawrence (2006), The impact of ice uptake of nitric acid on atmospheric chemistry, *Atmos. Chem. Phys.*, *6*, 225–235.

Wang, Q., D. J. Jacob, J. R. Spackman, A. E. Perring, J. P. Schwarz, N. Moteki, E. A. Marais, C. Ge, J. Wang, and S. R. H. Barrett (2013), Global budget and radiative forcing of black carbon aerosol: Constraints from pole-to-pole (HIPPO) observations across the Pacific, *J. Geophys. Res. Atmos.*, *119*, 195–206, doi:10.1002/2013JD020824.

Wespes, C., D. Hurtmans, C. Clerbaux, M. L. Santee, R. V. Martin, and P. F. Coheur (2009), Global distributions of nitric acid from IASI/MetOP measurements, *Atmos. Chem. Phys.*, *9*, 7949–7962.

Wolff, M. A., et al. (2008), Validation of HNO_3, $ClONO_2$, and N_2O_5 from the Atmospheric Chemistry Experiment Fourier Transform Spectrometer (ACE-FTS), *Atmos. Chem. Phys.*, *8*, 3529–3562, doi:10.5194/acp-8-3529-2008.

Zhang, L., D. J. Jacob, X. Liu, J. A. Logan, K. Chance, A. Eldering, and B. R. Bojkov (2010), Intercomparison methods for satellite measurements of atmospheric composition: Application to tropospheric ozone from TES and OMI, *Atmos. Chem. Phys.*, *10*, 4725–4739, doi:10.5194/acp-10-4725-2010.